Journal of Applied Polymer Science

Bio-inspired "green" nanocomposite using hydroxyapatite synthesized from eggshell waste and soy protein

Muhammad M. Rahman,[1] Anil N. Netravali,[1] Boniface J. Tiimob,[2] Vitus Apalangya,[2] Vijaya K. Rangari[2]

[1]Department of Fiber Science and Apparel Design, Cornell University, Ithaca, New York 14853
[2]Department of Material Science and Engineering, Tuskegee University, Tuskegee, Alabama 36088
Correspondence to: A. N. Netravali (E-mail: ann2@cornell.edu)

ABSTRACT: Eco-friendly and inexpensive "green" nanocomposites with enhanced functional performances were developed by combining nanoscale hydroxyapatite (HA) synthesized from eggshell waste (nEHA) and protein-based polymer extracted from defatted soybean residues. nEHA was synthesized from chicken eggshells using an energy efficient microwave-assisted wet chemical precipitation method. Transmission electron microscopy, X-ray diffraction, and energy-dispersive X-ray spectroscopy studies confirmed the nanometer scale (diameter: 4–14 nm and length: 5–100 nm) of calcium-deficient (Ca/P ratio ~1.53) needle-like HA. Uniform dispersion of nEHA in soy protein isolate (SPI) solution was obtained by modifying nEHA surface using a polyelectrolyte (sodium polyacrylate) dispersant via irreversible adsorption. Green nanocomposite films were prepared from SPI and surface-modified nEHA with the help of a natural plasticizer "glycerol" by solution casting. Significant improvements in tensile modulus and strength were achieved owing to the inclusion of uniformly dispersed nEHA in SPI sheets. Overall, this work provides a green pathway of fabricating nanocomposites using naturally occurring renewable polymer and inorganic moieties from eggshell waste that emphasizes the possibilities for replacing some petroleum-based polymers in packaging and other applications. © 2016 Wiley Periodicals, Inc. J. Appl. Polym. Sci. **2016**, *133*, 43477.

KEYWORDS: biopolymers and renewable polymers; composites; properties and characterization

Received 15 September 2015; accepted 25 January 2016
DOI: 10.1002/app.43477

INTRODUCTION

Soy protein, obtained after extracting oil from soybeans, has been explored before, as a bio-based polymer for use in sustainable green composites.[1–6] It is capable of forming numerous intra- and intermolecular bonds as well as engaging in physical interactions because of the presence of polar and functional groups in its amino-acids. Hence, it can form three-dimensional green structures with good mechanical properties.[7] Furthermore, soy protein is available throughout the world and has other benefits such as low cost, biodegradability, biocompatibility, environment friendliness, and yearly renewability. These advantages have made it highly attractive for use as an alternative to petroleum-based polymers which can reduce the carbon footprint and global warming significantly.[8–10] However, mechanical properties of protein-based polymers limit their utilization in various load-bearing structural applications.

Hydroxyapatite (HA), with chemical composition of $Ca_{10}(PO_4)_6(OH)_2$, is a very promising natural reinforcing material for polymers due to its high stiffness and strength. It is, in fact, the prime inorganic constituent (65–70%) of bone and hard tissue matrix that is indirectly bound to collagen through some non-collagenous proteins such as osteocalcin, osteopontin, or osteonectin in nanocrystal form.[11] It has two binding sites, Ca^{2+} and PO_4^{3-}, which possess affinity toward biological macromolecules such as proteins.[12] Synthetic HA has attracted much attention as a reinforcing material in biomedical applications because of its excellent functional properties including biocompatibility, osteoconductivity, nontoxicity, and bioactivity.[13,14] Moreover, synthesized HA at nanoscale can provide exceptional functional and mechanical properties similar to biological HA due to its large surface area to volume ratio and tunable ultrafine structure. As a result, nanoscale HA has been extensively utilized with various polymers to fabricate composites for bioapplications such as tissue scaffolds and bone regenerations.[15,16]

Commercially available soy protein is very inexpensive whereas nanoscale HA is expensive due to the use of high purity materials and reagents used to produce it. Since the bone-mimetic nanocomposites can contain more than 60% of HA, they can

Additional Supporting Information may be found in the online version of this article.

get very expensive. An alternative economical and environment-friendly "green" approach to synthesize HA would be to utilize biowastes such as eggshells, sea shells, bovine bones, and fish bones, etc., which are rich sources of calcium precursors, as raw materials.[17] For example, chicken eggshells contain a significant amount of calcium carbonate ($CaCO_3$; ~94%) bound in a very small amount of an organic matrix (~4%) consisting of collagen, sulfated polysaccharides and other polypeptides.[18] Every year, food processing industry in the United States, as a whole, throws away more than 4500 metric tons of chicken eggshells, in the landfills or even open land, without further treatment which causes significant environmental pollution.[19] Since it is a pure waste, eggshell has been considered a free and viable bio-derived source to synthesize inexpensive nanoscale HA while simultaneously reducing the eggshell waste.[20]

In earlier work, Lee *et al.* proposed that while biopolymers can interact with inorganic materials via electrostatic, van der Waals and/or hydrogen bonding, electrostatic interaction between the charged groups of both materials is the primary interaction.[12] Hassan *et al.* improved mechanical and thermal properties of soybean oil based unsaturated polyester (Polylite® 31325-00) resin by loading it with eggshell-based $CaCO_3$ nanoparticles.[21] About 14 and 27% improvements in compressive strength and compressive modulus, respectively, were observed in the resin with the incorporation of 2 wt % $CaCO_3$ nanoparticles. Tiimob *et al.* used eggshell derived β-$CaSiO_3$ nanoparticles to modify thermal and mechanical properties of bio-based epoxy resin system (Super sap® 100/1000).[22] Incorporation of just 3 wt % β-$CaSiO_3$ nanoparticles in the resin systems improved the flexural modulus (~33%) and flexural strength (~36%) significantly. In another study, the flexural strength, modulus, and toughness of bio-based epoxy resin system (Super sap® 100/1000) were significantly improved by 6–31, 11–37, and 10–36%, respectively, due to different amount of $CaCO_3$ nanoparticles loading (1–10 wt %).[23] However, these resins were not fully green.

In the present study, novel bio-inspired fully green composites from soy protein isolate (SPI) and eggshell-based nanoscale hydroxyapatite (nEHA) were prepared and characterized. Nothing has been reported yet on the utilization of bio-derived HA nanostructures in plant-based protein resins in the open literature with a view to producing a cost-effective and environment-friendly green composite for structural applications. In the first part of this article, a novel synthesis approach for obtaining nEHA from eggshell by energy-efficient microwave-assisted wet chemical precipitation method has been described. The wet chemical precipitation method was employed due to its ease of experimental operation and cost effectiveness. Also, microwave-assisted process can reduce the synthesis time significantly. In addition, the issue of nEHA dispersion, in water as well as in the resin, was resolved by coating the nEHA with sodium polyacrylate (NaPA). Better dispersion of nEHA can be achieved by chemical treatment which mitigates nanoparticle–nanoparticle attractions. Finally, uniformly dispersed nEHA was incorporated in soy protein resin to fabricate novel bio-based nanocomposites with enhanced mechanical and thermal properties.

EXPERIMENTAL

Materials

SPI was provided by Archer Daniels Midland, Decatur, IL. Raw white Eggshells were provided by American Dehydrated Foods, Atlanta, GA. Analytical grade sodium hydroxide (NaOH) pellets, glycerol (≥98% purity), ethanol (≥99.5% purity, absolute), nitric acid (~ 65% HNO_3), ammonium hydroxide (~28% NH_4OH), semiconductor grade phosphoric acid (~ 85% H_3PO_4), and NaPA (molecular weight ~2100) were purchased from Sigma-Aldrich Chemical, Allentown, PA. Milli-Q deionized (DI) water (resistivity, 18.2 MΩ.cm, Millipore RiOs and Elix water purification systems, Millipore Corporation, MA) was used throughout this research.

Synthesis of Nanoscale HA from Eggshell

nEHA was synthesized by using $CaCO_3$ from eggshell and H_3PO_4 as the sources of calcium and phosphate ions, respectively. As-received eggshells were first boiled in DI water overnight followed by pulverization in a "Waring" commercial kitchen blender to denature and decant organic materials from the heavier inorganic material settled at the bottom. The inorganic sample was dried under vacuum overnight at room temperature (RT) after washing with DI water and ethanol. The dried sample was pulverized again into fine eggshell powder ($CaCO_3$) and passed through a 20-μm mesh sieve.

Desired nEHA was synthesized from eggshell powder as follows: In the first step, 20 g of eggshell powder was added into an Erlenmeyer flask containing 28 mL of HNO_3 solution and magnetically stirred at 300 rpm for 30 min. This resulted into a yellowish $Ca(NO_3)_2$ slurry. In the second step, diammonium hydrogen phosphate [$(NH_4)_2HPO_4$, DAHP] powder was synthesized by transferring 60 mL of NH_4OH into a stoichiometric amount of H_3PO_4 (15 mL) at a rate of 1 mL/min using a micropipette. Precipitated white DAHP powder was then filtered and washed thoroughly using a mixture of DI water and ethanol (1:1 v/v). In the third step, 3 g of $Ca(NO_3)_2$ was dissolved in 100 mL of DI water and stirred for 10 min at 400 rpm at a temperature of 40 °C while 2.4 g of DAHP was dissolved in 60 mL of DI water, separately. Aqueous DAHP solution was added drop-by-drop into the $Ca(NO_3)_2$ solution at the rate of 3 mL/min. NH_4OH was then added to the reaction mixture to adjust the pH to 11 after which it was stirred for 5 min. Finally, the reaction mixture was put into a microwave (45 microwave power) in an isothermal condition of 80 °C for 15 min. After cooling to RT, the white precipitated material was collected, washed using a mixture of ethanol and DI water, and centrifuged to remove any residual polymer and ammonium nitrate. The washing procedure was repeated three times and dried which is herein termed as "as-synthesized nEHA." The following set of chemical reactions show the steps involved in the synthesis of nEHA:

$$CaCo_3(s) + 2HNO_3(aq) \rightarrow Ca(NO_3)_2(s) + CO_2(g) + H_2O(1)$$

$$2NH_4OH\ (aq) + H_3PO_4(aq) \rightarrow (NH_4)_2HPO_4(s) + 2H_2O(1)$$

$$10Ca(NO_3)_2(aq) + 6(NH_4)_2HPO_4 + 8NH4OH \rightarrow Ca_{10}(PO4)_6OH_2 + 10NH_4NO_3$$

Surface Coating on nEHA

Surface modification of as-synthesized nEHA was accomplished by coating it with NaPA to improve their dispersion in SPI resin.

The coating procedure was as follows: 1 g of as-synthesized nEHA was mixed with 50 mL of DI water and the suspension was stirred magnetically for 10 min to wet the particles. Then, the mixture was ultrasonicated (Q-500 Sonicator, Q-Sonica, CT) for 5 min at 50% amplitude and 30 s on-off pulse mode to break up the aggregated nEHA in the aqueous solution. Ten mL of 20-mM NaPA as anionic polyelectrolyte dispersant was added to the ultrasonicated aqueous suspension. The mixture was adjusted to pH of 6 using 1*N* HCl and stirred overnight at RT using a magnetic stirrer. Finally, the nEHA was washed with DI water to remove unadsorbed NaPA using centrifugation at 5000 rpm for 10 min. The washing procedure was repeated four times. Washed nEHA was dried in an oven at 80 °C overnight and is herein termed as "coated nEHA."

Fabrication of SPI-nEHA Nanocomposites

Green nanocomposites were prepared by combining coated nEHA as the inorganic reinforcing filler with SPI resin as the biopolymer. Coated nEHA (3, 5, and 10 wt %, based on SPI solid weight) with approximately 7 wt % NaPA (based on nEHA weight) dispersion was prepared in DI water and adjusted to pH of 10 using 1*N* NaOH. SPI was added to the colloidal dispersion at a ratio of 1:10 (SPI-nEHA: water) on a weight basis. Glycerol was added (5 wt % based on SPI solid weight) to SPI as a plasticizer to reduce the brittleness of the SPI sheets. The pH of the solution was adjusted to 10.5 ± 0.1 using 1*N* NaOH to open the protein molecules and denature them. The solution was then ultrasonicated for 2 min followed by stirring for 30 min at 80 °C to get a homogenous solution. This stage is termed "precuring." Teflon® coated glass plates (100 mm × 100 mm) were used to dry the precured solution in the sheet form. The solution on the glass plates was kept overnight at RT followed by drying in an air circulated oven at 65 °C for 2 h. Finally, hydraulic hot press (Carver Inc., Wabash, IN) was used to cure (cross-link) the dried SPI-nEHA nanocomposite sheets at a temperature of 140 °C for 10 min and a pressure of 8 MPa. Pure SPI sheets without nEHA were also fabricated using the same process. All sheets were conditioned at 60% RH and 21 °C for 24 h before carrying out any tests. SPI sheets incorporated with 3, 5, and 10 wt % coated nEHA are designated as SPI-nEHA3, SPI-nEHA5, and SPI-nEHA10 nanocomposites, respectively. Supporting Information Figure S1 shows the schematic diagram of the formation of nanoscale HA-reinforced soy protein-based green nanocomposites.

Characterization of as-Synthesized nEHA

Phase analysis of as-synthesized nEHA nanostructures was carried out by X-ray diffraction (XRD) using a Scintag theta–theta powder diffractometer (PAD X, Scintag, Cupertino, CA). The Cu-*K*α radiation ($\lambda = 1.54$ Å) was used at a voltage of 40 kV and a current of 30 mA. The diffraction patterns were recorded in the range of 20–60° Bragg angles (2θ) at a scan rate of 3° min^{-1} with a step size of 0.03°. The interplaner distance (d_{hkl}) in different crystal directions of nEHA was calculated from Bragg's equation[24]: $d_{hkl} = \frac{\lambda}{2\sin\left(\frac{\pi}{180}\right)}$, where λ is the wavelength of Cu-Kα radiation and is the diffraction angle. The crystallite size (τ_{hkl}) of nEHA in the direction perpendicular to the crystal face of (hkl) was estimated from the obtained diffraction peaks using the Scherrer equation[24]: $\tau_{hkl} = \frac{K\lambda}{\beta_{hkl}\cos\theta}$; where K is the broadening constant and chosen as 0.9[24] and β_{hkl} is the full width at half-maximum intensity of diffraction peaks corresponding to (hkl) lattice plane. The crystallinity index (X_c) corresponding to (002) reflection of nEHA was calculated by using the relationship: $\beta_{002}\sqrt[3]{X_c} = k_a$; where k_a is a constant equal to 0.24.[25] The lattice parameters (a- and c-axes) of nEHA crystals were calculated by using the relationship among lattice constant, Miller indices (h, k, l), and d-spacing: $\frac{1}{d_{hkl}} = \sqrt{\frac{4}{3}\cdot\frac{h^2+hk+k^2}{a^2} + \frac{l^2}{c^2}}$; while unit cell volume (V) was determined using the calculated lattice parameters: $V = \frac{\sqrt{3}a^2c}{2}$. The specific surface area (SSA) of as-synthesized nEHA was determined by nitrogen sorption analysis in 11-point area mode on a BET (Brunauer-Emmett-Teller) surface area analyzer from Quantachrome Instruments (Model: NOVA 2200*e*, Boynton Beach, Florida). Particle size and morphology of as-synthesized nEHA were observed using a JEOL-2010 high-resolution transmission electron microscope (TEM; HRTEM, JEOL USA, Peabody, MA) at 200 kV. To prepare specimens for HRTEM imaging, as-synthesized nEHA was ultrasonicated in ethanol for 5 min at RT and a drop was placed onto a carbon-coated copper grid and allowed to dry before HRTEM observation. Electron diffraction pattern for single crystal was also taken by the JEOL HRTEM. Particle size distribution (PSD) of nEHA was determined using ImageJ software (National Institutes of Health) by measuring a total of more than 100 particles from TEM micrographs. Energy dispersive X-ray spectroscopy (EDX) was performed using a Bruker Energy dispersive spectrometer coupled with Tescan Mira3 FESEM to find out the molar ratio of calcium/phosphorus of as-synthesized nEHA.

Characterization of Coated nEHA

Attenuated total reflection-Fourier transform infrared (ATR-FTIR) spectra and thermogravimetry combined with Zeta (ζ) potential measurements were used to confirm nEHA nanoparticle coating by NaPA. ATR-FTIR spectra were recorded in the range of 600–4000 cm^{-1} wavenumbers using a Nicolet Magna 560 spectrometer (Nicolet Instrument Corporation, Madison, WI). Each spectrum was an average of 256 scans with a resolution of 2 cm^{-1}. Thermogravimetric analysis (TGA) of specimens was carried out on a TG analyzer (TGA-2050, TA Instruments, DE) using a flow of 60 mL/min nitrogen gas. TGA scans were conducted in the temperature range of 30–600 °C at a constant heating rate of 10 °C/min. ζ potentials and PSDs of as-synthesized and NaPA coated nEHA in aqueous suspensions were measured using a Malvern Zetasizer Nano ZS100 device (Malvern Instruments, Malvern, UK) with irradiation from a 633-nm He-Ne laser. ζ potential was calculated from measured electrophoretic mobility using the Smoluchowski approximation.[26] Dynamic light scattering (DLS) technique was performed using the same instrument to determine PSD in aqueous suspensions. In DLS method, the intensity of light was scattered at an angle of 173° by an avalanche photodiode.

Characterization of SPI-nEHA Nanocomposites

The optical transmittance of specimens was measured using a UV–visible spectrophotometer (Lambda 35, Perkin Elmer, Norwalk, CT). The wavelengths were selected between 400 and 800 nm with a resolution of 1 nm. Moisture content (MC) of specimens was measured according to a method described by Rhim *et al.*[27] Tensile properties such as Young's modulus, tensile strength and fracture strain of the specimens were measured according to ASTM D882-02 using an

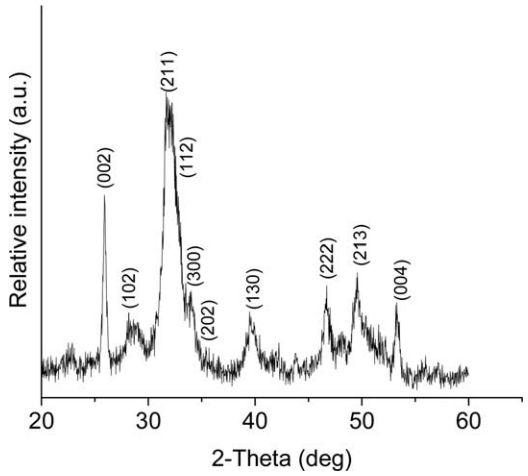

Figure 1. Representative XRD pattern of as-synthesized nEHA.

Instron universal tensile testing machine (Model: 5566, Canton, MA). Specimens with dimensions of 10 × 30 mm^2 were tested at the strain rate of 1 min^{-1}. A minimum of 10 specimens of each composition were tested to perform the statistical analyses. TEM images of thin sections of nanocomposites were obtained using FEI Tecnai T12 TEM (Hillsboro, OR) to show the dispersion of nEHA in the specimens. The specimens were sliced into ultrathin sections using an ultramicrotome (Leica EM UC7, Buffalo Grove, IL). These sections were placed on a carbon-coated copper grid, individually, before TEM observation. LEO 1550 field emission scanning electron microscope (FESEM, Cambridge, UK) was used to analyze the fracture surface of the specimens at 3-kV accelerating voltage. ATR-FTIR, TG, and EDX analyses of the sheet specimens were carried out as mentioned in Physico-Chemical Properties of as-Synthesized nEHA and Surface Modification of as-Synthesized nEHA sections. Analysis of variance (ANOVA) followed by multiple comparison tests using Tukey-Kramer's HSD at 95% confidence level were performed for statistical evaluations. Statistical analyses were performed using JMP software by SAS Institute (Cary, NC).

RESULTS AND DISCUSSION

Physico-Chemical Properties of as-Synthesized nEHA

A representative XRD pattern of the as-synthesized nEHA is presented in Figure 1. All crystallographic information from experimental XRD pattern was compared with standards by the Joint Committee on Powder Diffraction and Standards (JCPDS). All the peaks were matched closely with those of PDF standard card (00-009-0432) patterns and corresponded to polycrystalline hexagonal lattice cell with a space group of $P6_3/m$. As shown in the Figure 1, the diffraction peak at 25.88° corresponding to the (002) Miller plane was the most isolated one. The relative intensity of the (002) reflection (66%) was much higher in comparison to the standard XRD pattern of stoichiometric HA (36%) which reveals that the proposed synthesis favors nEHA crystal growth along the *c*-axis (JCPDS card no. 00-009-0432).[28] The other observation was the broadening of the peak at around 32° which indicates small crystalline size of nEHA.[25] The diffraction peaks at 25.88° and 32.90° were selected for the calculation of the crystallite sizes since the (002) Miller plane corresponds to the crystal growth following the *c*-axis while the (300) Miller plane corresponds to the crystal growth following *a*-axis. The crystallite size was found to be larger in the [002] crystallographic direction than that of the [300] direction which implies rod or needle-like structure of the synthesized nEHA.[13] Crystallinity index of nEHA was found to be 35% which is comparable to previously reported data.[25] Table I shows the summary of calculated values from the XRD pattern of as-synthesized nEHA. These values were consistent with the previously reported data for synthesized HA.[13,25]

The SSA of as-synthesized nEHA by nitrogen sorption (BET) analysis was found to be 100.6 m^2/g. The high SSA of as-synthesized nEHA is advantageous as it provides desirable interface for stress transfer in a polymeric composite. The corresponding volume-surface mean diameter (D_{BET}) of as-synthesized nEHA was calculated using the empirical equation assuming equivalent spherical morphology: $D_{BET} = \frac{6}{\rho \times SSA}$; where ρ is the particle density.[29] A theoretical density of 3.16 g/cm^3 for HA was used in all calculations.[29] The estimated volume–surface mean diameter from the BET method was found to be 20 nm which corroborates completely with the crystallite size along *a*-axis obtained from the XRD studies.

Figure 2 shows HRTEM images along with the selected area electron diffraction (SAED) pattern of as-synthesized nEHA. As shown in Figure 2(a), the micrograph depicts an irregular needle-like shape of primary nEHA with a broad size distribution in length (typically from 5 to 100 nm) and diameter (typically from 4 to 14 nm). The HRTEM observations corroborate the XRD analysis which revealed *c*-axis crystal growth in nEHA. Although some immature particles were observed [Figure 2(a)] as spherical shapes, the number was very small compared to the irregular needle-like nEHA. Irregularly shaped reinforcement, in fact, can be better in composites as they allow better mechanical interlocking with the polymeric resin.[11] However, a high degree of agglomeration was observed owing to the large surface area of nEHA. High SSA provides strong attractive forces between nEHA allow forming agglomeration and entanglements, due to irregular shape, if not suitably dispersed. Figure 2(b) displays the crystalline structure of as-synthesized nEHA with interplanar spacings of 0.34 and 0.26 nm corresponding to spacings along the (002) and (300) planes, respectively, which are in agreement with the XRD analysis. The corresponding SAED pattern taken

Table I. Summary of Values Calculated from XRD Pattern of as-Synthesized nEHA

Sample	Lattice parameters (Å)		Unit cell volume (Å^3)	Crystallite size (nm)		Crystallinity index (%)
	a, *b*	*c*		τ_{002}	τ_{300}	$X_{c\ (002)}$
HA from Eggshell	9.46	6.88	533.21	28.0	19.6	35

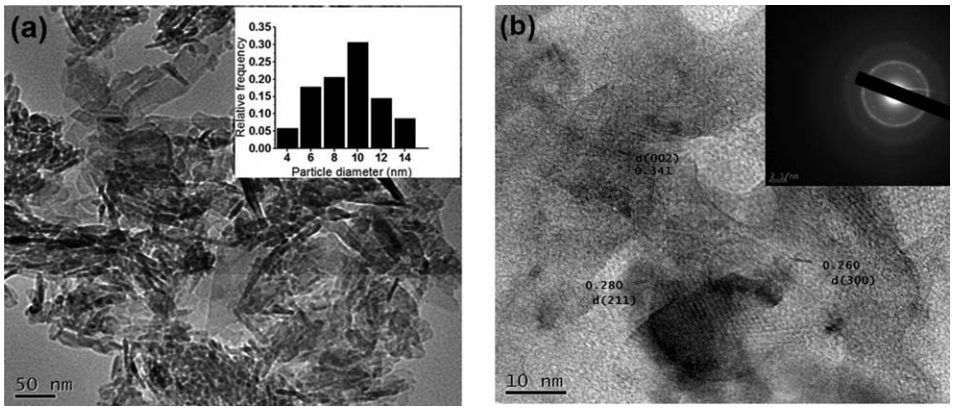

Figure 2. HRTEM micrographs showing (a) as-synthesized nEHA with inset of particle diameter frequency distribution plot, (b) crystalline structure and inter-planer distances corresponding to *(002)* and *(300)* planes with inset of corresponding electron diffraction pattern of nEHA.

from a single nEHA structure reveals significant crystallinity index as exhibited by the spotty diffraction rings which are also consistent with the XRD results [inset of Figure 2(b)].

Surface Modification of as-Synthesized nEHA

While high SSA provides desirable interfacial interaction to transfer stress in a polymeric composite, it also causes excessive agglomerations which can act as failure precursors in a composite. To obtain the true benefits of nanoparticle addition, i.e. higher properties, uniform dispersion of the nEHA is critical. In a solution casting approach, stable and uniform dispersion can be achieved by manipulating the surface engineering of as-synthesized nEHA. Nanoparticle–nanoparticle interactions in an aqueous medium are determined by mainly two opposite forces: van der Waals attraction and electrostatic double layer repulsion.[30,31] These two forces determine whether the net interaction between nanoparticles is repulsive or attractive and, hence, determines the colloidal stability. The electrostatic double layer repulsive interaction can be tuned by modification at the particle's surface using a suitable dispersant mediator. In the present study, the surface of the as-synthesized nEHA was coated by NaPA, a water-soluble polyelectrolyte dispersant, through adsorption, to increase the electrostatic double layer repulsion between particles and prevent their aggregation. Optimum coating of NaPA onto nEHA surfaces was determined to avoid any negative effects of having either insufficient or excess amount of the dispersant in the composites.

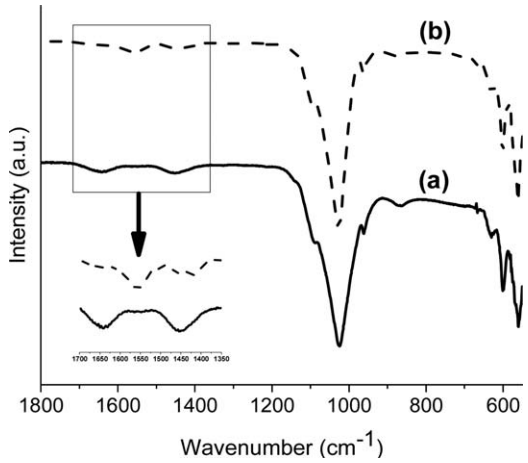

Figure 3. FTIR spectra of (a) as-synthesized nEHA and (b) coated nEHA.

The NaPA coating on the nEHA surface was confirmed through ATR-FTIR spectroscopy. Figure 3(a,b) shows the ATR-FTIR spectra of as-synthesized and coated nEHA. Both spectra contain the characteristic peaks at 1091, 1026, 962, 610, and 560 cm^{-1} for phosphate stretching vibration modes (υ_3, υ_3, υ_1, υ_4, and υ_2 of PO_4^{3-}, respectively).[25,32] The band at 1450 cm^{-1} is from dissolved CO_2 during the wet chemical synthesis of nEHA which was liberated during the NaPA adsorption process in nEHA.[32] As shown in Figure 3(b), the absorption peaks at 1560 and 1410 cm^{-1} have been observed in the spectrum of coated nEHA which can be attributed to the asymmetric and symmetric vibration modes of the COO^- group, respectively.[33,34] Along with these bands, a weak absorption at 1465 cm^{-1} can be assigned to the CH_2 bending mode of NaPA.[34] These similar bands were also observed in NaPA (Supporting Information Figure S3). However, these bands were not present in the spectrum of as-synthesized nEHA as shown in Figure 3(a).

The amount of NaPA coating onto the surface of as-synthesized nEHA was calculated by TGA. Figure 4 shows representative TGA thermograms of NaPA, as-synthesized nEHA and coated nEHA. As shown in Figure 4, the decomposition of NaPA was observed within a temperature range above 400–550 °C with a weight loss of about 50%. Similarly, an abrupt single-step weight loss of 6–7% was observed for the coated nEHA compared to as-synthesized nEHA. This can be attributed to desorption and decomposition of NaPA molecules adsorbed on nEHA surfaces. Single-step weight loss also indicates a monolayer coating formation of NaPA onto the nEHA.[35] It is worth mentioning here that the weight loss observed up to 200 °C can be attributed to physisorbed and chemisorbed water.

Mean zeta (ζ) potentials of as-synthesized and coated nEHA as a function of pH were measured to quantify the electrostatic double-layer repulsive charge of nEHA particles in solutions that determine the most stable and uniform aqueous dispersions. The ζ-potential data are presented in Figure 5. A rough criterion for stability of particles in colloidal systems is that the ζ-potential value of the particles must be greater than ± 30

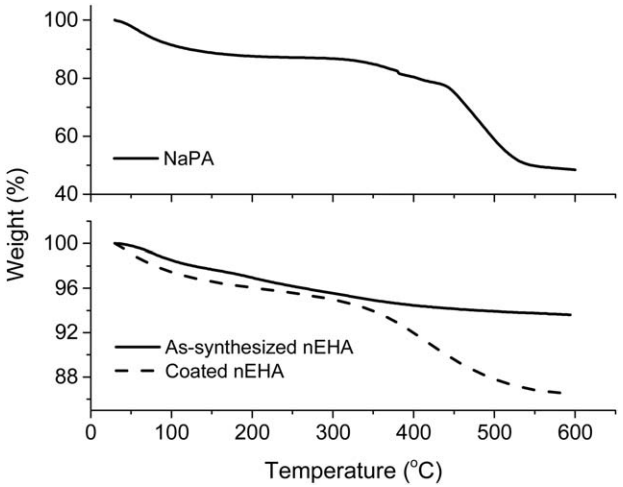

Figure 4. TGA thermograms of NaPA, as-synthesized and coated nEHA.

mV.[3] As can be seen in Figure 5, the ζ-potential of coated nEHA has a higher negative surface charge than that of the as-synthesized nEHA at each pH value which indicates an increased electrostatic double layer repulsion force because of irreversible adsorption of NaPA. The ζ-potential of nEHA became more negative above its isoelectric point with increasing pH for both samples. At pH of about 10, the largest mean ζ-potential value was found for coated nEHA (ca. −50 mV). This value is significantly higher than the critical value for stable and uniform suspension as well as capable of preventing the approach of charged nEHA particles and hence, preventing large agglomeration in the system. Also, the irreversible adsorption of NaPA onto nEHA surfaces causes the isoelectric point (IEP) to shift to the stronger acidic side (∼pH 2.5). During the adsorption process, exposed hydroxyl groups on nEHA surfaces are liberated into solution by the anionic domains of polyacrylate[29,36] and hence, will result in a shift of IEP to a more acidic pH. The irreversible adsorptions of NaPA on as-synthesized nEHA surfaces involves an ion exchange mechanism between phosphate ions and carboxylate (COO^-) groups of polyacrylate at the solid-solution interfaces while COO^- groups and Ca^{2+} sites of nEHA may irreversibly interact by electrostatic interactions.[29,36] Besides, an adsorbed polymer chain can be changed from extended coil conformation to train-loop-tail conformation which increases the steric hindrance from the repulsion of loops and tails of adsorbed polymer.[29,37]. In train-loop-tail model, polymer molecules adsorbed by particles at an interface can form a layer consisting of trains (polymer in direct contact with the particles), loops (polymer sections coming back to the contact surface) and tails (polymer chain ends). Thus, ion-exchange mechanism, electrostatic interactions, and steric hindrance phenomenon can explain the irreversible adsorption of NaPA and stabilization of nEHA particles in aqueous solution.

The effect of pH and coating on PSDs of nEHA in various aqueous suspensions by DLS measurements is presented in Supporting Information Figure S5. The volume-weighted mean size[38] of as-synthesized nEHA agglomerates in DI water was ca. 1416 nm with a broad range in PSD between 825 and 2670 nm. A substantial reduction in mean agglomerate size was observed for coated nEHA suspensions maintained at pH of 10. The volume-weighted average mean size of coated nEHA became about 402 nm while PSD ranged between 52 and 860 nm. To estimate the degree of agglomeration in the suspension, the average agglomeration number (AAN) was calculated using the method described by Hackley.[39] AAN is defined as the average number of primary particles contained in the agglomerate and is calculated from the equation[39]: $\mathrm{AAN}=\left(\frac{D_{50}}{D_{\mathrm{BET}}}\right)^3(1-\varepsilon)$, where D_{50} is the volume–median size obtained from PSD by DLS measurement, D_{BET} is the volume–surface mean diameter as calculated previously from BET analysis of sorption isotherms and ε is the fractional porosity of the agglomerate approximated as 0.4.[29] The AAN value for as-synthesized nEHA was calculated to be about 2.1×10^5 while the value in the case of coated nEHA suspensions (ca. 4.8×10^3) was smaller by about two orders of magnitude. Substantial reduction in particle sizes and AAN was established by a combined effect of ultrasonication along with a polyelectrolyte coating in an alkaline medium. The formation and destruction of cavities during ultrasonication provides a shear force on the agglomerates that facilitates overcoming the van der Waals attractions holding them together. At the same time, polyelectrolyte on nEHA increases electrostatic repulsive charge between nanoparticles so that they do not re-agglomerate after ultrasonication and, hence, form a stable dispersion.

Characterization of SPI-nEHA Nanocomposites

SPI sheets were fabricated through the formation of various intramolecular and intermolecular cross-links between polypeptide chains during precuring and curing processes. The most common covalent cross-links in SPI are intermolecular disulfide linkages which are formed by the oxidation of the sulfhydryl groups of two cysteine residues under heat.[40] Alkali treatment coupled with thermal processing during precuring and curing stage can also result in the racemization of amino acid residues

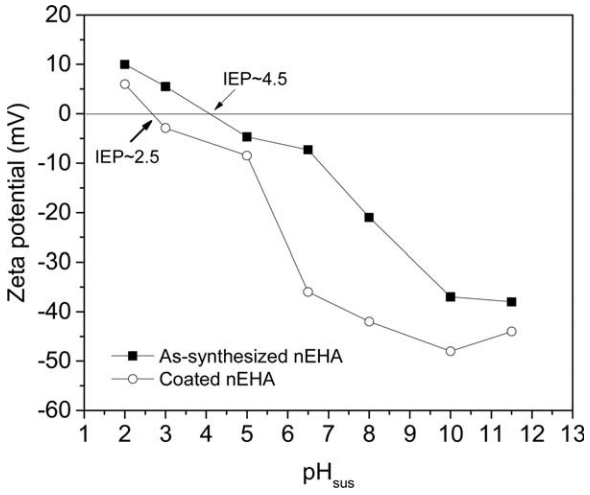

Figure 5. Mean ζ-potential of as-synthesized and coated nEHA as a function of pH.

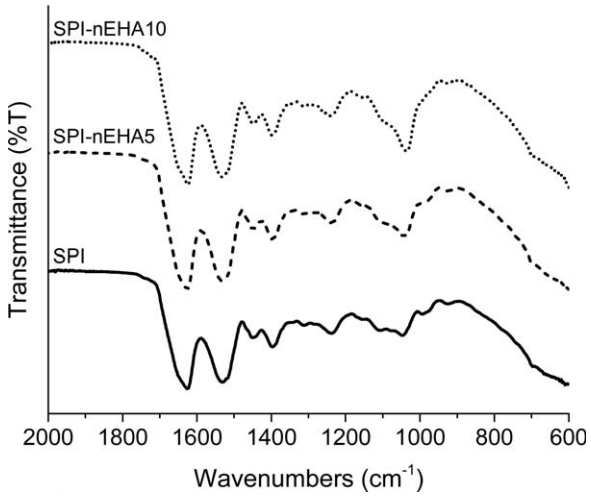

Figure 6. Representative ATR-FTIR spectra of SPI sheets and SPI-nEHA nanocomposites.

and facilitate some covalent crosslinking interactions.[41] For example, dehydroalanine can be formed by the loss of side chains beyond the β-carbon in amino acid residues. The dehydroalanine residues can react with various nucleophilic groups such as ε-amino group in lysine and sulfhydryl group of cysteine residues to form lysinoalanine and lanthionine crosslinks. Thus, the resulting intramolecular and intermolecular covalent crosslinks during the precuring and curing stages are stable that facilitate to form a three-dimensional solid structure.

Figure 6 shows the representative ATR-FTIR spectra of SPI and SPI-nEHA nanocomposite sheets. As shown in the figure, the peak at 1026 cm^{-1} for the phosphate stretching mode (υ_3 of PO_4^{3-}) of nEHA moved to 1042 cm^{-1} in the SPI-nEHA nanocomposite spectrum. Also, the absorption increased with higher nEHA loading. Mere physical interactions between SPI and nEHA as characterized by the υ_3 vibration mode of PO_4^{3-} in nEHA may be sufficient for this shift as the υ_3 vibration mode of phosphate has been found by others to be in a broad range of 1020–1045 cm^{-1}.[42,43] The band 1048 cm^{-1} wavenumber in SPI are attributed to C = O stretching for glycerol plasticization.[44] Hence, the peak at 1042 cm^{-1} for nEHA merged with the C = O stretching (1048 cm^{-1} wavenumber) in SPI resulting in higher peak intensity, with increased nEHA loading in SPI. It was also observed that the presence of nEHA in SPI did not change protein conformations as amide I, amide II, and amide III band positions at 1624, 1530, and 1241 cm^{-1}, respectively, were found to be similar to pure SPI.

The effect of incorporating coated nEHA on the optical transmittance of SPI sheet was determined using UV–visible spectrophotometer and is presented in Supporting Information Figure S6. Transparency value (TV) at unit light path length of the nanocomposite sheets was calculated by the equation[9]: $TV = (-\log T_{600})/d$, where, T_{600} is the transmittance at 600 nm and d is sheet thickness in mm. TV was taken at 600 nm as it is the approximate average wavelength of the visible light region. The higher the TV, the lower is the transparency. Incorporation of coated nEHA in SPI resin decreases the transparency of the sheets. Pure SPI sheets had a TV of 7.4 ± 1.3 whereas SPI-nEHA10 nanocomposite sheets showed a maximum value of 28.6 ± 3.1. Even, the TV of SPI-nEHA10 nanocomposites was significantly higher compared to that of SPI-nEHA5 nanocomposites (14.6 ± 1.6). At higher loading, nEHA in SPI nanocomposites aggregated together due to lower interparticle distances and formed larger units.[3] These larger units increased the light scattering and led to the significant increase of the TV which indicates the increased opaqueness of the sheets with increased nEHA content in the nanocomposites.

Table II shows MC values of SPI sheets and SPI-nEHA nanocomposite sheets after conditioning the specimens. As shown in Table II, the variations in MC among sheets were not significant ($P > 0.05$) and were varied in the range of 9–11%. Table II also shows the variations in tensile properties as a function of coated nEHA content. Typical stress–strain behavior of SPI and SPI-nEHA nanocomposite sheets in tensile mode are presented in Supporting Information Figure S7. As seen from data in Table II, Young's modulus and tensile strength of SPI sheets increased, and fracture strain decreased with nEHA loading. Young's modulus or stiffness improved with a maximum enhancement of about 130% at 10 wt % of nEHA loading while an enhancement of 60% in tensile strength was observed at SPI-nEHA5 nanocomposites compared to SPI sheets. This, however, was accompanied by a substantial drop in fracture strain making SPI-nEHA nanocomposite sheets brittle. Fracture strain dropped by 80% at 10 wt % nEHA loading in comparison to pure SPI sheets. Statistical analysis based on one-way ANOVA revealed significant differences in tensile properties between SPI sheets and SPI-nEHA nanocomposites sheets ($P < 0.05$). Tukey-Kramer all pairs HSD tests also showed that incorporation of nEHA in SPI sheets had the significant effect. The tensile properties fall into clearly different groups between SPI and SPI/nEHA sheets.

An optimum amount of NaPA can improve the interfaces between nEHA and SPI resin. NaPA can be irreversibly adsorbed

Table II. Tensile Properties and Moisture Content of SPI and SPI-nEHA Nanocomposite Sheets

Specimen sheets	Young's modulus (MPa)	Tensile strength (MPa)	Fracture strain (%)	Moisture content (%)
SPI	923 ± 127[a]	25 ± 2.5[a]	18 ± 3.0[a]	10.4 ±0.6[a]
SPI-nEHA3	1486 ± 135[b]	35 ± 3.5[b]	12 ± 2.6[b]	9.9 ± 0.8[a]
SPI-nEHA5	1737 ± 192[b]	41 ± 3.5[c]	7.2 ± 1.7[c]	10.3 ± 0.6[a]
SPI-nEHA10	2147 ± 207[c]	38 ± 2.8[bc]	4.3 ± 1.4[d]	10.6 ± 0.4[a]

Means not connected by same letter superscripts are significantly different at 95% confidence level through Tukey-Kramer HSD test.

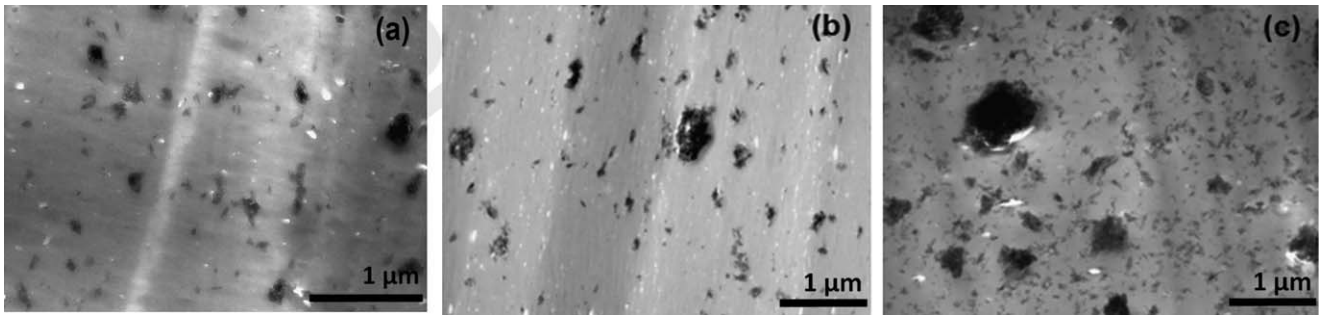

Figure 7. TEM images showing the dispersion state of nEHA in (a) SPI-nEHA3, (b) SPI-nEHA5, and (c) SPI-nEHA10 nanocomposite sheets.

onto the nEHA surface while it can form intermolecular interactions with SPI via hydrogen bond or dipole–dipole interactions. However, it seems to have no significant effect on the mechanical properties of composites by optimum NaPA coating which is very less in terms of soy protein matrix. Rather, the dispersion at the microscopic level is one of the important factors that can significantly improve the mechanical properties of nanocomposites.[15,45] Figure 7 shows the dispersion state of nEHA in SPI-nEHA3, SPI-nEHA5, and SPI-nEHA10 nanocomposite sheets. Uniform dispersion of 3 and 5 wt % nEHA in SPI resin as can be seen in Figure 7(a,b). This low loading level provided more sites to facilitate polymer–nanoparticle interaction at the interface due to higher surface area of nEHA particles.[3] This facilitates a more efficient stress transfer and leads to the improvement in stiffness. However, microscopic level dispersion became difficult to achieve in SPI-nEHA10 nanocomposites as shown in Figure 7(c). During processing, the interparticle distance decreased for higher loading causing flocculation of nEHA which remained in the form of large aggregates in the sheets. More agglomerations with increased aggregate sizes were observed in SPI-nEHA10 nanocomposites which corroborates with the TV of nanocomposites discussed earlier. SPI resin is globular and cannot intercalate into the nEHA agglomerates while only the outside of the agglomerates can be bonded to the polymer. These agglomerates can act as stress concentrators in composites which causes early shear slippage of individual particles within the agglomerates resulting in decreased strength.[46] However, the modulus or stiffness was found to be a function of loading as it increased with the loading amount.

Figure 8 shows FESEM images of the fracture surfaces of SPI, SPI-nEHA5, and SPI-nEHA10 nanocomposite sheets after the uniaxial tensile test. The fracture surface of the SPI sheet was much smoother and featureless indicating less interruption during failure propagation as shown in Figure 8(a). Figure 8(b,c) is the fracture surface images of SPI-nEHA5 and SPI-nEHA10 nanocomposites, respectively, that show greater surface roughness with continual crack deflection and propagation in different fracture planes. Deviation of fracture plane from crack initiation plane can be attributed to the presence of distributed nEHA. The presence and distribution of nEHA in the fracture surfaces of SPI-nEHA nanocomposite sheet was confirmed by EDX mapping analysis (Supporting Information Figure S8). EDX mapping analysis of SPI sheet showed no trace of any Ca or P elements while the homogeneous presence and distribution of Ca and P confirmed the uniformly embedded nEHA throughout the nanocomposite.

SPI-nEHA nanocomposites and their properties can be compared with other nanocomposites.[3–5,21,22,47–49] Bio-based inorganic nanoparticles such as $CaCO_3$,[3,21] $CaSiO_3$,[22] nanoclay,[5] and halloysite nanotubes[47] incorporated polymeric composites have properties comparable to the SPI-nEHA nanocomposites in this study. The aforementioned nanoparticles have been incorporated in some green resins such as soy protein[3,5] and polyvinyl alcohol (PVA)[47] resin while the mechanical properties were lower in comparison to SPI-nEHA nanocomposites. For example, 5% $CaCO_3$ nanoparticles loaded SPI showed a Young's modulus of 1055 MPa and tensile strength of 28 MPa[3] while 5% glutaraldehyde cross-linked soy protein concentrate (SPC) had a Young's modulus of 969 MPa and tensile strength of 28.5 MPa, respectively with the addition of 5% nanoclay.[5] Halloysite nanotubes loading at 20% improved the Young's modulus of PVA to 466 MPa, about twice that of control PVA.[47] Comparable mechanical properties were also observed when bacterial cellulose (BC)[48] or microfibrillated

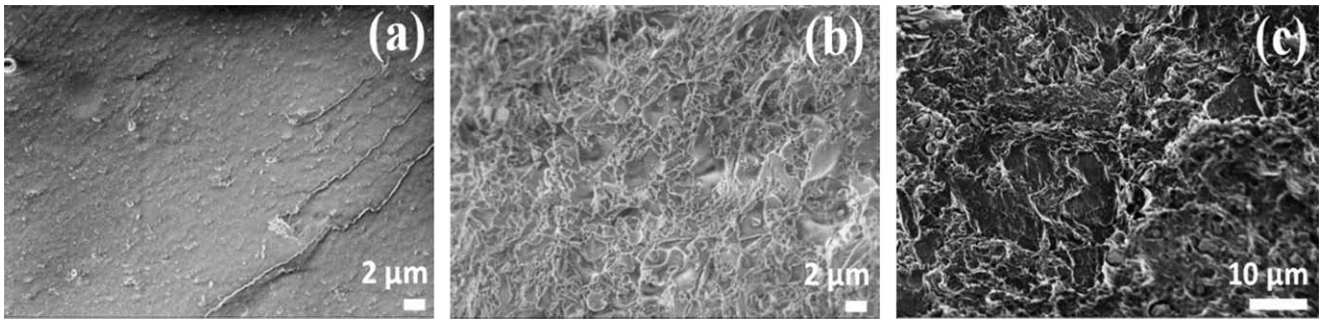

Figure 8. FESEM images showing the fracture surfaces of (a) SPI sheet, (b) SPI-nEHA5 and (c) SPI-nEHA10 nanocomposite sheets after uniaxial tensile test.

cellulose[4] were incorporated in biodegradable resins. For example, Young's modulus and tensile strength of PVA with 50% BC by volume were found to be 1590 and 32.6 MPa, respectively.[48] Young's modulus of SPC was found to be 1816 MPa with the addition of 30% of micro/nano-sized bamboo fibrils.[4] Properties of SPI-nEHA nanocomposites in the present study are easily comparable with starch-based polymeric resin as mentioned by Verbeek and Bier *et al.*[50] Even the properties of some engineering polymers such as polyurethane, polystyrene, etc., are comparable with the SPI-nEHA nanocomposite as presented by Bayer *et al.*[51]

CONCLUSIONS

This study introduces a very inexpensive, sustainable, and environment-friendly green nanocomposite produced using soybean processing byproducts and eggshell waste that could be used in many applications. Nanoscale hydroxyapatite from eggshell waste was successfully synthesized by energy-efficient microwave-assisted wet chemical precipitation and then incorporated in soy-based resin by ensuring uniform dispersion by a polyelectrolyte coating. The coated nanoscale hydroxyapatite showed as effective filler for soy-protein-based biopolymer in terms of improvement in functional properties of the nanocomposites. However, loading above 5% of nEHA decreased the material homogeneity and functionality due to the agglomeration tendency. Still, the fabricated nanocomposite can replace some synthetic polymers to fabricate polymeric materials with significantly lower carbon footprint. They can be further reinforced with high strength fibers such as liquid crystalline cellulose to fabricate green composites.

ACKNOWLEDGMENTS

The authors acknowledge NSF-CREST grant (1137681) for funding this work. They also acknowledge the use of Cornell Center for Materials Research (CCMR) facilities supported by NSF (award no. DMR-1120296).

REFERENCES

1. Song, F.; Tang, D. L.; Wang, X. L.; Wang, Y. Z. *Biomacromolecules* **2011**, *12*, 3369.
2. Lubasova, D.; Mullerova, J.; Netravali, A. N. *J. Appl. Polym. Sci.* **2015**, *132*, DOI: 10.1002/app.41852.
3. Rahman, M. M.; Netravali, A. N.; Tiimob, B. J.; Rangari, V. K. *ACS Sustain. Chem. Eng.* **2014**, *22*, 2329.
4. Huang, X.; Netravali, A. *Compos. Sci. Technol.* **2009**, *69*, 1009.
5. Huang, X.; Netravali, A. *Compos. Sci. Technol.* **2007**, *67*, 2005.
6. Kumar, R.; Anandjiwala, R. D. *J. Appl. Polym. Sci.* **2012**, *124*, 3132.
7. Silva, N. H. C. S.; Vilela, C.; Marrucho, I. M.; Freire, C. S. R.; Neto, C. P.; Silvestre, A. J. D. *J. Mater. Chem. B* **2014**, *22*, 3715.
8. Netravali, A. N.; Chabba, S. *Mater. Today* **2003**, *66*, 22.
9. Rahman, M. M.; Ho, K.; Netravali, A. N. *J. Appl. Polym. Sci.* **2015**, *132*, DOI: 10.1002/app.41291.
10. Rahman, M. M.; Netravali, A. N. *ACS Sustain. Chem. Eng.* **2014**, *22*, 2318.
11. Šupová, M. *J. Mater. Sci. Mater. Med.* **2009**, *20*, 1201.
12. Lee, W. H.; Loo, C. Y.; Zavgorodniy, A. V.; Ghadiri, M.; Rohanizadeh, R. *RSC Adv.* **2013**, *33*, 4040.
13. Pramanik, N.; Imae, T. *Langmuir* **2012**, *28*, 14018.
14. Song, B.; Xu, Q.; Wang, C.; Xu, S.; Zhang, H. *J. Appl. Polym. Sci.* **2015**, *133*, 42871, DOI: 10.1002/app.42871.
15. Singh, M. K.; Shokuhfar, T.; Gracio, J. J.; de, A.; de Sousa, A. C. M.; Fereira, J. M. D. F.; Garmestani, H.; Ahzi, S. *Adv. Funct. Mater.* **2008**, *18*, 694.
16. Khajavi, R.; Abbasipour, M.; Bahador, A. *J. Appl. Polym. Sci.* **2016**, *133*, DOI: 10.1002/app.42883.
17. Wu, S. C.; Tsou, H. K.; Hsu, H. C.; Hsu, S. K.; Liou, S. P.; Ho, W. F. *Ceram. Int.* **2013**, *39*, 8183.
18. Rivera, E. M.; Araiza, M.; Brostow, W.; Castaño, V. M.; Díaz-Estrada, J. R.; Hernández, R.; Rodríguez, J. R. *Mater. Lett.* **1999**, *41*, 128.
19. Yoo, S.; Hsieh, J. S.; Zou, P.; Kokoszka, J. *Bioresour. Technol.* **2009**, *100*, 6416.
20. Hassan, T. A.; Rangari, V. K.; Jeelani, S. *Int. J. Nano Biomater.* **2014**, *55*, 103.
21. Hassan, T. A.; Rangari, V. K.; Jeelani, S. *J. Appl. Polym. Sci.* **2013**, *130*, 1442.
22. Tiimob, B. J.; Rangari, V. K.; Jeelani, S. *J. Appl. Polym. Sci.* **2014**, *131*, DOI: 10.1002/app.40867.
23. Tiimob, B. J.; Jeelani, S.; Rangari, V. K. *J. Appl. Polym. Sci.* **2016**, *133*, DOI: 10.1002/app.43124.
24. Klug, H. P.; Alexander, L. E. In X-ray Diffraction Procedures: For Polycrystalline and Amorphous Materials, 2nd ed.; Wiley Interscience: New York, **1974**; Vol. *1*, Chapter 3.
25. Puvvada, N.; Panigrahi, P. K.; Pathak, A. *Nanoscale* **2010**, *22*, 2631.
26. White, B.; Banerjee, S.; O'Brien, S.; Turro, N. J.; Herman, I. P. *J. Phys. Chem. C* **2007**, *111*, 13684.
27. Rhim, J. W.; Gennadios, A.; Weller, C. L.; Cezeirat, C.; Hanna, M. A. *Ind. Crops Prod.* **1998**, *88*, 195.
28. Zhang, Y.; Lu, J. *Cryst. Growth Des.* **2008**, *88*, 2101.
29. Chen, C. W.; Oakes, C. S.; Byrappa, K.; Riman, R. E.; Brown, K.; TenHuisen, K. S.; Janas, V. F. *J. Mater. Chem.* **2004**, *14*, 2425.
30. Derjaguin, B.; Landau, L. *Prog. Surf. Sci.* **1993**, *43*, 30.
31. Verwey, E. J. W.; Overbeek, J. T. G. *J. Colloid Sci.* **1955**, *1010*, 224.
32. Costa, D. O.; Dixon, S. J.; Rizkalla, A. S. *ACS Appl. Mater. Interfaces* **2012**, *44*, 1490.
33. Bertoni, E.; Bigi, A.; Falini, G.; Panzavolta, S.; Roveri, N. *J. Mater. Chem.* **1999**, *99*, 779.
34. Li, H.; Tripp, C. P. *Langmuir ACS J. Surface Colloids* **2004**, *2020*, 10526.
35. Lin, Y.; Chen, H.; Chan, C. M.; Wu, J. *Macromolecules* **2008**, *41*, 9204.
36. Skinner, J. C.; Prosser, H. J.; Scott, R. P.; Wilson, A. D. *Biomaterials* **1986**, *77*, 438.

37. Fleer, G. J.; Stuart, M. A. C.; Scheutjens, J. M. H. M.; Cosgrove, T.; Vincent, B. In Polymers at interfaces, 1st Ed.; Chapman and Hall: London, **1993**; Chapter 4.
38. Merkus, H. G. In Particle Size Measurements: Fundamentals, Practice, Quality, 1st ed.; Springer: Netherlands, **2009**; Vol. *1*.
39. Hackley, V. A. *NIST Spec. Publ.* **2000**,
40. Singh, H. *Trends Food Sci. Technol.* **1991**, *22*, 196.
41. Gerrard, J. A. *Trends Food Sci. Technol.* **2002**, *13*, 391.
42. Uysal, I.; Severcan, F.; Evis, Z. *Ceram. Int.* **2013**, *39*, 7727.
43. Chang, M. C.; Tanaka, J. *Biomaterials* **2002**, *23*, 4811.
44. Lodha, P.; Netravali, A. N. *Ind. Crops Prod.* **2005**, *21*, 49.
45. Liu, Q.; de Wijn, J. R.; van Blitterswijk, C. A. *Biomaterials* **1997**, *18*, 1263.
46. Rahman, M. M.; Hosur, M.; Zainuddin, S.; Jahan, N.; Miller-Smith, E. B.; Jeelani, S. *J. Compos. Mater.* **2015**, *49*, 759.
47. Qiu, K.; Netravali, A. N. *Polym. Compos.* **2013**, *34*, 799.
48. Qiu, K.; Netravali, A. N. *J. Mater. Sci.* **2012**, *47*, 6066.
49. Zhao, Z.; Shan, W.; Zhang, Y.; Li, X.; Ma, J.; Yan, Y. *J. Appl. Polym. Sci.* **2012**, *125*, 2502.
50. Verbeek, C. J. R.; Bier, J. M. In A Handbook of Applied Biopolymer Technology: Synthesis, Degradation and Applications; Sharma, S. K.; Mudhoo, A, Eds.; RSC Green Chemistry (Book 12); RSC Publishing: UK, **2011**; Chapter 7.
51. Bayer, I. S.; Guzman-Puyol, S.; Heredia-Guerrero, J. A.; Ceseracciu, L.; Pignatelli, F.; Ruffilli, R.; Cingolani, R.; Athanassiou, A. *Macromolecules* **2014**, *47*, 5135.